The ortho-para transition, confinement and self-diffusion of H_2 in three distinct carbide-derived carbons by quasi- and inelastic neutron scattering

Riinu Härmas[1*], *Rasmus* Palm[1,2], *Miriam* Koppel[1], *Laura* Kalder[1], *Margarita* Russina[3], *Heisi* Kurig[1], *Eneli* Härk[1,3], *Jaan* Aruväli[4], *Indrek* Tallo[1], *Jan P.* Embs[5], and *Enn* Lust[1]

[1]Institute of Chemistry, University of Tartu, Ravila 14a, 50411 Tartu, Estonia
[2]Department of Applied Physics, KTH Royal Institute of Technology, SE-106 91 Stockholm, Sweden
[3]Helmholtz-Zentrum Berlin für Materialien und Energie, Hahn-Meitner-Platz 1, 14109 Berlin, Germany
[4]Department of Geology, University of Tartu, Ravila 14a, 50411 Tartu, Estonia
[5]Laboratory for Neutron Scattering and Imaging, Paul Scherrer Institute, Forschungsstrasse 111, CH-5232, Villigen PSI, Switzerland

Abstract. Microporous carbon materials are promising for hydrogen storage due to their structural variety, high specific surface area, large pore volume and relatively low cost. Carbide-derived carbons are highly valued as model materials because their porous structure is fine-tuned through the choice of the precursor carbide and the synthesis route. This study investigates H_2 adsorption in three carbide derived carbons with well-defined pores and pore size distributions with quasi- and inelastic neutron scattering methods. Concerning previous studies, a wider neutron energy transfer window is investigated, and a detailed quantitative evaluation of the graphitic structure is presented. The graphitic structure of the carbon is shown to influence the speed of the ortho-to-para transition of H_2. Namely, the ortho-para transition was the slowest in carbon derived from TiC, which also had the smallest average stacking size of graphene layers. The possibility to inhibit the ortho-para transition in cryo-adsorption devices is sought after to mitigate the evaporation of H_2 during storage. In addition, the self-diffusion of H_2 in different timescales is detected in carbon derived from Mo_2C, demonstrating the usefulness of obtaining data in a wide energy window.

1 Introduction

Currently, hydrogen storage is one of the most expensive components in implementing entire hydrogen value chains [1]. In order to increase the density of hydrogen, it needs to be stored either at high pressure (300–700 bar) or at a very low temperature (20 K). Both methods result in a significant drop in the overall energy efficiency of the hydrogen value chain. Porous materials have attracted interest as hydrogen storage materials, since these can help to alleviate the problem of the unfavourable compressibility factor of H_2 at low temperatures and high pressures. Although low temperatures and pressures higher than atmospheric pressure are still needed for H_2 storage in cryo-adsorption systems, the conditions for hydrogen storage are much milder in the case of porous materials [2]. It has been shown that the optimal conditions for using porous materials for hydrogen storage lie in the temperature range of 77–150 K, and the storage pressure is up to approximately 250 bar. At 80 K and in the pressure range from 100 to 200 bar, cryo-adsorption vessels have been shown to contain up to 20% more H_2 compared with the corresponding cryo-compression vessels, which do not contain adsorbents [3].

Carbide-derived carbons (CDCs) have been shown to be excellent model materials to analyze the effect of porous structure on performance of the carbon in specific applications (e.g. H_2 storage, charge storage in supercapacitors) [4,5]. CDCs are synthesized from inorganic carbides (e.g., TiC) through the reaction with chlorine at high temperature, typically 700–1200 °C, where the formed chloride is removed in gas flow. Thus, from the carbide structure only the chemically pure carbon, noted as CDC, is left behind. It has been previously shown that the average graphene platelet size in these types of materials is in the range of 2.3–8.2 nm [6], and the average pore shapes depend on the precursor carbide [7] and the chlorination temperature used [8]. In a previous quasi-elastic neutron scattering (QENS) study on the instrument FOCUS at PSI, the transport properties of H_2 in the pores of CDCs derived from SiC, Mo_2C and TiC was investigated in the energy range from -2 to 2 meV. As a result, the sub-nanometer pores of C-SiC were shown to contain almost immobile hydrogen (i.e. solid-like) even at a relatively high temperature of 120 K [5]. In this study, the Quasi-elastic neutron scattering (QENS) data of H_2 diffusing in the pores of CDCs derived from SiC, Mo_2C and TiC is revisited to investigate a larger transfer energy window with respect to the previous study. The aim is to

* Corresponding author: riinu.harmas@ut.ee

investigate the ortho-para transition band of H_2 and to verify if fast H_2 diffusion can be detected in the broader energy window.

2 Experiment

The precursor carbides and the chlorination temperatures of the studied carbon materials can be seen in Table 1.

Table 1. Overview of the main synthesis parameters of the studied CDCs.

	Precursor carbide	**Chlor. *T* °C**	**Ref.**
C-TiC	TiC	950	[7,9]
C-SiC	SiC	1000	[7,10]
C-Mo_2C	Mo_2C	1000	[7,11]

X-ray diffraction patterns were measured using D8 Advance diffractometer (Bruker) with Cu Kα radiation and Bragg-Brentano geometry. To obtain structural parameters, the data were fitted with the Ruland and Smarsly algorithm [12] using the CarbX software (https://www.uni-giessen.de/CarbX) [13].

QENS measurements of H_2 adsorbed in C-TiC, C-SiC, and C-Mo_2C were performed at Paul Scherrer Institute in Villigen, Switzerland, on the cold neutron time-of-flight spectrometer FOCUS [14] with incident neutron wavelength of 5.02 Å and the elastic energy resolution of 100 μeV. Data were obtained in the energy transfer range of E = −37 meV to 2 meV and scattering vector, Q, range of 0.4–2.5 $Å^{-1}$ (corresponding scattering angle range 2θ 18–174°). A cylindrical aluminium sample holder with an inner cylinder was used for all samples. The outer diameter of the sample was 1.02 cm, and the inner diameter of the sample was 0.555 cm. Empty sample holder and vanadium measurements were performed for background subtraction and data correction.

Before the QENS measurement, all three CDCs were outgassed to remove moisture and other adsorbed species. After the outgassing process, the CDCs were transferred into the sample holder in a glovebox. The signal from the outgassed samples was measured in the temperature range of 10–120 K. H_2 with normal ortho-para content (3:1) was dosed in the sample holder at 77 K until the pressure reached the $p_{H2,load}$ value (Table 2). The adsorption equilibrium was established and, thereafter, the sample holder was hermetically sealed and, thus, disconnecting it from the gas dosing apparatus, and data were measured at different temperatures ranging from 10 to 120 K. H_2 pressure in the sample holder varied according to the reached adsorption equilibrium at each experimental temperature point as the sample holder was hermetically sealed during the experiment.

Table 2. Conditions for hydrogen loading, $p_{H2,load}$, is the H_2 pressure in the sample holder at 77 K, n_{H2}, mmol g^{-1} is the total amount of H_2 per mass of carbon in the sample holder.

CDC adsorbent	$p_{H2,load}$ **bar**	n_{H2} **mmol g^{-1}**	***w*% of H_2 in sample at 20 K**
C-TiC	0.011	2.0	0.4%
C-SiC	0.011	2.4	0.48%
C-Mo_2C	0.087	1.2	0.24%

Data reduction, which included normalization with vanadium, corrections for detector efficiency and subtraction of background, was performed with the DAVE 2.4 software. [15] Binning of the scattering data were conducted in the whole energy transfer range, from dE = –37 meV to 2 meV, with step size 0.047 meV; Q was binned over the entire range as one slice. Since Q was summed over all detectors, the reported dynamic incoherent structure factors $S(Q,E)$ are noted as intensity $S(E)$, in the following text.

The intensity of signal from hydrogen, $S_{H2}(E)$, was obtained by subtracting the intensity of signal of degassed carbon, $S_C(E)$, from the total intensity $S(E)$.

$$S_{H2}(E) = S(E) - S_C(E) \quad (1)$$

To investigate the diffusion of H_2 in multiple timescales, i.e. to detect whether multiple quasi-elastic broadening signals are convoluted in $S_{H2}(E)$, the quasi-elastic broadening of $S_{H2}(E)$ was analysed. The $S_{H2}(E)$ was symmetrised based on the neutron energy gain side and fitted in the energy range from E = –30 meV to 30 meV with equation 2.

$$S_{model}(E) = A_0\,\delta(E) + A_1\,L(E,\Gamma_1) + A_2\,L(E,\Gamma_2) + y_0 \quad (2)$$

where $S_{model}(E)$ is the model scattering signal, $\delta(E)$ is the Dirac delta function describing the elastic scattering, A_0 is the fraction of elastic and A_1 and A_2 are the fractions of quasi-elastic scattering signals, L is the Lorentzian function which describes the quasi-elastic component mathematically, Γ is the half width at half maximum of the quasi-elastic component, and y_0 is the background. The characteristic times for rotational diffusion were calculated based on the Γ_1 and Γ_2 values by converting energy units (1 meV = $2.42 \cdot 10^{11}$ Hz).

3 Results and discussion

3.1 Ortho-para transition of H_2

The rotational energy levels are given by

$$E_J = \mathrm{B}\,J\,(J+1) \quad (3)$$

where J is the rotational quantum number and B = 7.37 meV. The free quantum rotor energy of the

transition from the lower energy para level to the higher energy ortho level (p→o, $J = 0 \rightarrow 1$) is 14.7 meV [16,17].

The para-ortho transition band is seen when the H_2 is adsorbed strongly in the carbon material, i.e. due to adsorption, the H_2 molecule struck by the neutron is not able to diffuse freely and therefore, undergoes rotational excitation [18–20]. The detection of p→o transition band has been seen as evidence of very strongly adsorbed H_2 in the porous material [21]. The ortho to para (o→p, $J = 1 \rightarrow 0$), i.e. a reverse transition could be investigated in the energy transfer window available in this study. At room temperature, the ortho to para ratio of hydrogen is about 3:1, but para form will become prevalent at low temperatures. The spin conversion process from ortho to para H_2 is exothermic releasing 535 kJ kg^{-1} of heat, meaning that a rapid o→p conversion could result in desorption and evaporation of the adsorbed H_2 [22]. Therefore, it is of interest to stabilize the H_2 adsorbed in ortho state.

H_2 adsorbed in C-TiC, a o→p transition band near $E = -14$ meV is visible at 10 K (Fig. 1a). However, no o→p transition band is detected at low hydrogen coverages ($p_{H2,load} \leq 87$ mbar) in C-SiC and Mo_2C in the investigated temperature range (Fig. 1b-c). The pore size distributions of C-SiC and C-TiC are very similar [5], so the porous structure alone cannot explain why the o→p transition band was seen for H_2 adsorbed in C-TiC, but not for H_2 adsorbed in C-SiC and C-Mo_2C at 10 K. As the temperature is increased to 50 K, a slight quasi-elastic broadening becomes visible in the $S(E)$.

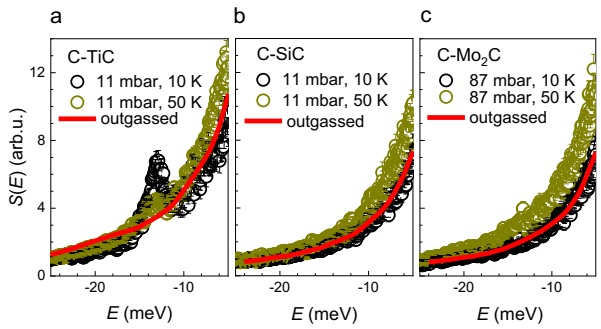

Fig. 1. The intensities, $S(E)$, in the o→p energy transfer range. (a) C-TiC at $p_{H2,load} = 11$ mbar, (b) C-Mo_2C at $p_{H2,load} = 87$ mbar and (c) C-SiC at $p_{H2,load} = 11$ mbar. The red lines correspond to the intensities of the corresponding outgassed carbons, $S_C(E)$.

The main structural aspect differentiating C-TiC from other studied carbon material is the lack of graphitic ordering. Namely, the main difference lies in the 002 reflections in the X-ray diffraction patterns (Fig. 2), which is related to stacking of graphene layers.

The average stacking size, L_c, average interlayer spacing, a_3, and the average graphene layer extent, L_a, were estimated based on the X-ray diffraction patterns (Table 3). The algorithm that was used for this analysis (See part 2) calculates the L_c and a_3 parameters based on the shape of the 002 reflection and the L_a parameter from the shape of the 10 reflection [12]. Based on these parameters, the C-TiC material shows a more disordered structure compared to the other investigated CDCs. L_c values show the most significant difference between the investigated materials, less than 1 nm for C-TiC and 12.7 nm for C-SiC. Also, the L_a value is almost two times smaller compared to that of C-SiC and C-Mo_2C.

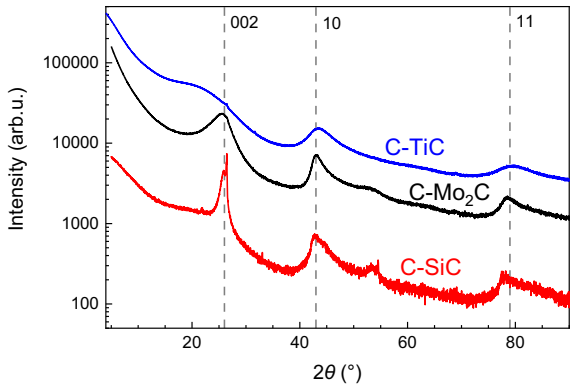

Fig. 2. The X-ray diffraction patterns of studied materials (noted in Figure). The dashed lines represent the reflections along with their assignment.

Table 3. Main structural parameters of CDCs calculated based on XRD patterns with Ruland and Smarsly algorithm [12].

CDC	L_c nm	a_3 nm	L_a nm
C-TiC	0.6	0.38	4.5
C-SiC	12.7	0.36	7.1
C-Mo_2C	2.7	0.35	8.3

L_c - average stacking size, a_3 - average interlayer spacing, L_a, average graphene layer extent

In this study, a normal mixture of ortho and para hydrogen was dosed into the carbon at 77 K, i.e. the ratio of ortho to para H_2 corresponded to 3:1. If by the time of measurement, there was a negligible amount of ortho-H_2 in the carbon, also the ortho-para transition band would not be visible as seen for C-SiC and C-Mo_2C. Namely, at low temperatures (<80 K), the thermodynamically more stable para form should become prevalent, but the carbon's structure influences the kinetics of the transition from o→p. It has been shown that depending on the carbon material, the o→p transition can be as slow as 0.4% h^{-1} [23] or as fast as ~140% h^{-1}. [24] This difference has been attributed to paramagnetic sites at the edges of graphitic planes, which can catalyse the o→p transition.

Therefore, since C-TiC is the most disordered, it should contain more edges, defects, etc., which can catalyse the o→p transition. However, since no o→p transition was seen in the more graphitic C-SiC and C-Mo_2C at 10 K, the o→p conversion must have been faster in these materials.

In addition, preferred adsorption of o-H_2 can occur in some pores. The physisorption energy is a sum of the isotropic and anisotropic terms of the adsorption

potential. While the isotropic term is the same for both ortho and para species, the anisotropic term can be different. Namely, the energy of the o-H_2 rotational levels can be lowered or raised due to anisotropic term, while the para level is left unchanged. This indicates that due to the decrease in the o-H_2 energy level in specific anisotropic adsorption sites, o-H_2 can be preferably bound to these sites and conversion to p-H_2 would then be less likely [16].

Recently, in the study of Terry et al. [19], the specific adsorption of o-H_2 in carbon materials was detected. These adsorption sites were attributed to the smallest pores (pore width, w = 0.4 nm) or some specific adsorption sites with a disorder-induced curvature. So, it might be the case that for low surface coverage, H_2 in C-TiC is adsorbed in the ortho state and not convert to para form easily. Thus, despite the anticipated conversion of most of the ortho species to para species already before the start of the neutron scattering measurement, an appreciable amount of hydrogen is still left in the ortho state in the pores in C-TiC. Thus, the existence of o→p transition band proves the existence of o-H_2 still in the pores which alludes to the H_2 rotation being strongly affected by the anisotropic adsorption potential in these pores.

This explanation is also supported by the fact that the o→p band seen in C-TiC was centred at approx. dE = −13 meV (Fig.1), instead of dE = −14.7 meV seen for freely rotating H_2. This deviation refers to strong anisotropic adsorption potential in the pores of C-TiC.

3.2 Quasi-elastic broadening, i.e. H_2 diffusion

The H_2 diffusion was recently seen to occur in multiple different timescales in the pores of carbon materials. [25] This has increased the interest to investigate the quasi-elastic broadening component of $S(E)$ in a wide energy transfer window. From the investigated CDC materials, a wide temperature-dependant quasi-elastic broadening was detected in the $S_{H2}(E)$ in the C-Mo_2C material at temperatures over 25 K (Fig. 3a). This could refer to fast self-diffusion of H_2 that could occur in mesopores and be also related to multilayer adsorption.

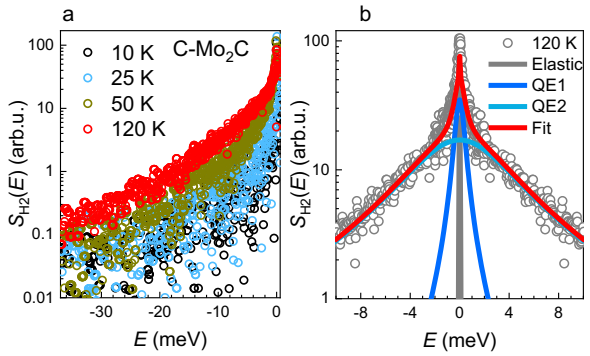

Fig. 3. (a) The $S_{H2}(E)$ of hydrogen in C-Mo_2C ($p_{H2,load}$ = 87 mbar). (b) The deconvolution of $S_{H2}(E)$ of C-Mo_2C ($p_{H2,load}$ = 87 mbar) at 120 K. QE1 is the quasi-elastic intensity related to the slower self-diffusion, and QE2 is the quasi-elastic intensity related to the faster self-diffusion of H_2.

To investigate the existence of self-diffusion at different timescales, the $S_{H2}(E)$ was fitted with equation 2. The successful fit was obtained using two Lorentzian functions in addition to the resolution function (Fig. 3b). This demonstrates that H_2 self-diffusion with speed faster than previously reported exists in C-Mo_2C.

Assuming the rotational diffusion mechanism, the characteristic times were calculated based on the half-width half-maxima of the quasi-elastic broadening components (Table 4). It can be seen how the residency times between rotational jumps decrease with the increase in temperature. Further measurements are needed to ascertain the mechanism of H_2 diffusion by investigating the Q dependence of the quasi-elastic broadening signal.

Table 4. Assuming rotational diffusion, the characteristic residency times of H_2, τ_{rot}, in the pores of C-Mo_2C was calculated.

T K	QE1, τ_{rot} ps	QE2, τ_{rot} ps
50	18.5 ± 1.5	1.0 ± 0.1
70	6.9 ± 0.2	0.5 ± 0.1
120	4.8 ± 0.2	0.5 ± 0.1

Conclusions

The graphitic structure of the porous carbon material affected the transition from ortho to para hydrogen. C-TiC was the most disordered of the studied CDC materials and the only one for which the o→p transition band of H_2 was seen at 10 K. Moreover, there were evidence of H_2 rotation being strongly affected by the anisotropic adsorption potential in the pores of C-TiC. This finding can have an impact on the practical application since it would be preferable to keep hydrogen in the ortho state. Namely, storing H_2 in the ortho form would help avoid heat generation that comes from ortho to para transition during hydrogen storage in cryo-adsorption systems.
In addition, H_2 self-diffusion in different timescales was seen in the case of C-Mo_2C at temperatures over 25 K. This gives the incentive to study the self-diffusion of H_2 in the pores of carbon material in a wider energy transfer window in the future.

Acknowledgements

The sample holder was designed by Dr. Dirk Wallacher from Helmholtz-Zentrum Berlin für Materialien und Energie Probenumgebung. Paul Scherrer Institute is thanked for beamtime on FOCUS. The authors would like to thank Marek Bartkowiak for his help during the experiment at PSI. This research was supported by the EU through the European Regional Development Fund (Centers of Excellence, TK141 20142020.4.01.15-0011 and TK117 3.2.0101e0030); European Spallation Source: Estonian Participation in ESS Instrument

design, development and building and application for scientific research SLOKT12026T and SLTKT16432T and Graduate School of Functional materials and technologies receiving funding from the European Regional Development Fund in University of Tartu, Estonia. This work has been also partially supported by Estonian Research Council Institutional Research Grant IUT20e13 and personal research grants PUT55 and PUT1033.

References

1. V. Dias, M. Pochet, F. Contino, H. Jeanmart, Front. Mech. Eng., **6** (2020)
2. D.P. Broom, C.J. Webb, K.E. Hurst, P.A. Parilla, T. Gennett, C.M. Brown, R. Zacharia, E. Tylianakis, E. Klontzas, G.E. Froudakis et al., Appl. Phys. A, **122** (2016**)**
3. G. Petitpas, P. Bénard, L.E. Klebanoff, J. Xiao, S. Aceves, Int. J. Hydrog. Energy., **39** (2014)
4. V. Presser, M. Heon, Y. Gogotsi, Adv. Funct. Mater., **21** (2011)
5. R. Härmas, R. Palm, M. Russina, H. Kurig, V. Grzimek, E. Härk, M. Koppel, I. Tallo, M. Paalo, O. Oll et al., Carbon, **155** (2019)
6. R. Härmas, R. Palm, H. Kurig, L. Puusepp, T. Pfaff, T. Romann, J. Aruväli, I. Tallo, T. Thomberg, A. Jänes et al., *C*, **7** (2021)
7. H. Kurig, M. Russina, I. Tallo, M. Siebenbuerger, T. Romann, E. Lust, Carbon, **100** (2016)
8. R. Palm, R. Härmas, E. Härk, B. Kent, H. Kurig, M. Koppel, M. Russina, I. Tallo, T. Romann, J. Mata et al., Carbon, **171** (2021)
9. H. Kurig, T. Romann, A. Jänes, E. Lust, ECS Trans., **25** (2010)
10. M. Käärik, M. Arulepp, M. Karelson, J. Leis, Carbon, **46** (2008)
11. A. Jänes, T. Thomberg, H. Kurig, E. Lust, Carbon, **47** (2009)
12. W. Ruland, B. Smarsly, J Appl Cryst, J Appl Crystallogr, **35** (2002)
13. T. Pfaff, M. Simmermacher, B.M. Smarsly, J Appl Crystallogr, **51** (2018)
14. J. Mesot, S. Janssen, L. Holitzner, R. Hempelmann, J. Neutron Res., **3** (1996)
15. R.T. Azuah, L.R. Kneller, Y. Qiu, P.L.W. Tregenna-Piggott, C.M. Brown, J.R.D Copley, R.M. Dimeo, J Res Natl Inst Stand Technol, **114** (2009)
16. K. Fukutani, T. Sugimoto, Prog. Surf. Sci., **88** (2013)
17. I.F. Silvera, Rev. Mod. Phys., **52** (1980)
18. P.A. Georgiev, D.K. Ross, P. Albers, A.J. Ramirez-Cuesta, Carbon, **44** (2006)
19. L.R. Terry, S. Rols, M. Tian, I. da Silva, S.J. Bending, V.P. Ting, Nanoscale, **14** (2022)
20. P.A. Georgiev, D.K. Ross, A. De Monte, U. Montaretto-Marullo, R.A.H. Edwards, A.J. Ramirez-Cuesta, M.A. Adams, D. Colognesi, Carbon, **43** (2005)
21. C.I. Contescu, D. Saha, N.C. Gallego, E. Mamontov, A.I. Kolesnikov, V.V. Bhat, Carbon, **50** (2012)
22. K.T. O'Neill, S. Al Ghafri, B. da Silva Falcqão, L. Tang, K. Kozielski, M.L. Johns, Chem Eng Process, **184** (2023)
23. P.R. Kubik, W.N. Hardy, H. Glattli, Can. J. Phys, **63** (1985)
24. C.A. Swenson, J. Chem. Phys., **18** (1950)
25. M. Koppel, R. Palm, R. Härmas, M. Russina, V. Grzimek, J. Jagiello, M. Paalo, H. Kurig, M. Månsson, O. Oll et al., Carbon, **197** (2022)